Modifying the hydrophobic nature of MAF-6

Gutierrez-Sevillano, J.J.; Martin-Calvo, A.; Dubbeldam, D.; Calero, S.

DOI
10.1016/j.seppur.2021.119422

Publication date
2021

Document Version
Final published version

Published in
Separation and Purification Technology

Separation and Purification Technology 277 (2021) 119422

Contents lists available at ScienceDirect

Separation and Purification Technology

journal homepage: www.elsevier.com/locate/seppur

Modifying the hydrophobic nature of MAF-6

Juan José Gutiérrez-Sevillano [a,1], Ana Martin-Calvo [a,1,*], David Dubbeldam [b,1], Sofia Calero [c,a,1,*]

[a] Department of Physical, Chemical, and Natural Systems, University Pablo de Olavide, Sevilla, Spain
[b] Van't Hoff Institute for Molecular Sciences, University of Amsterdam, Amsterdam, The Netherlands
[c] Department of Applied Physics, Eindhoven University of Technology, Eindhoven, The Netherlands

ARTICLE INFO

Keywords:
Adsorption
Water
Alcohol
NaCl
MAF-6
Molecular simulations

ABSTRACT

Using a combination of molecular simulations techniques, we evaluate the structural tunability of the metal azolate framework with zeolitic RHO topology, MAF-6. Two mechanisms are explored to induce hydrophilicity to this hydrophobic material. The study at a molecular level of water adsorption takes place under a variety of conditions. On a first step, we consider water mixtures containing benzene or alcohols, paying special attention to the effect of the size of the alcohol molecules. On a second approach, we analyse the effect of small weight percentages of salt into the MAF-6 on the water adsorption. We first validate the accuracy of the host–guest interactions by reproducing experimental data. A new set of Lennard-Jones parameters for the interaction water- MAF-6 is also provided. The water adsorption behaviour of MAF-6 is studied in terms of adsorption isotherms, heats of adsorption, radial distribution functions, hydrogen bonds formation, and water distribution inside the material. We found that the presence of long molecules of alcohols favours the water adsorption at low values of pressure by smoothing the phase transition of water withing the MAF-6. On the other hand the addition of salt to the structure creates additional adsorption sites for water enhancing its adsorption, while reducing the saturation capacity of the material since the presence of salt reduces the accessible pore volume.

1. Introduction

Tuning porous materials is a resource that has been widely exploited to optimize the performance of these materials for specific purposes. Among this type of materials, the tailorability of carbon materials, zeolites, and metal–organic frameworks are the most studied.

Variations on the template of carbon materials, used during the synthesis process, allow controlling the structural properties of these materials and open the possibility of incorporating organic, inorganic, or biomaterials inside the porous channels or on the surface of the carbon walls. These functionalizations affect not only to the specific surface area or the electronic properties of the materials, but also enhance their performance on many applications, as semiconductors, catalysts, sensors, or adsorbents [1–6].

During- and post-synthesis approaches have been applied to zeolites affecting their properties. Depending on the crystal topology, size, morphology, and the nature of the heteroatoms and the cations used for charge compensation, the catalytic properties of zeolites can be modified, influencing their thermal stability, selectivity, or lifetime [7–11].

Metal–organic frameworks (MOFs) is probably the most studied, and not yet done, family of porous materials in terms of tunability. Since their first discovery, it was clear that the huge amount of possible metal–ligand combinations would lead to an enormous amount of available material [15,16]. During synthesis it is possible to manipulate the crystallization, structure, and morphology of MOFs by adjusting compositional parameters (solvent, pH, metal source, reactant concentration, molar ratio of the reactants) or process parameters (time, temperature, pressure, heating source). This is of interest for scaling-up the synthesis of MOFs for their industrial application at large scale [17]. In electrosynthesized MOFs, the applied potential seems to have a key role in determining the morphology, thickness, and electrochemical properties of MOFs, regulating the electrocatalytic activity, surface accumulation, and sensing ability of the material [18]. The addition of functional groups together with other post-synthesis modifications lead to an expansive amount of materials with different size, morphology, or surface properties, enhancing their potential for selected applications [19]. Multiple functional groups can be added to the ligands such as amino-, halo-, hydroxy-, ether, thiol, etc [20,21]. Post-synthetic modifications include exchanges of organic linkers [22,23] and metal ions [24,25], conversion from a highly ordered crystalline material toward a heterogeneous porous material [26], or opening of coordination sites by the addition of extra ligands to the structure

* Corresponding authors.
E-mail addresses: amarcal@upo.es (A. Martin-Calvo), s.calero@tue.nl (S. Calero).
[1] All authors contributed equally to this work.

https://doi.org/10.1016/j.seppur.2021.119422
Received 28 April 2021; Received in revised form 28 July 2021; Accepted 1 August 2021
Available online 8 August 2021

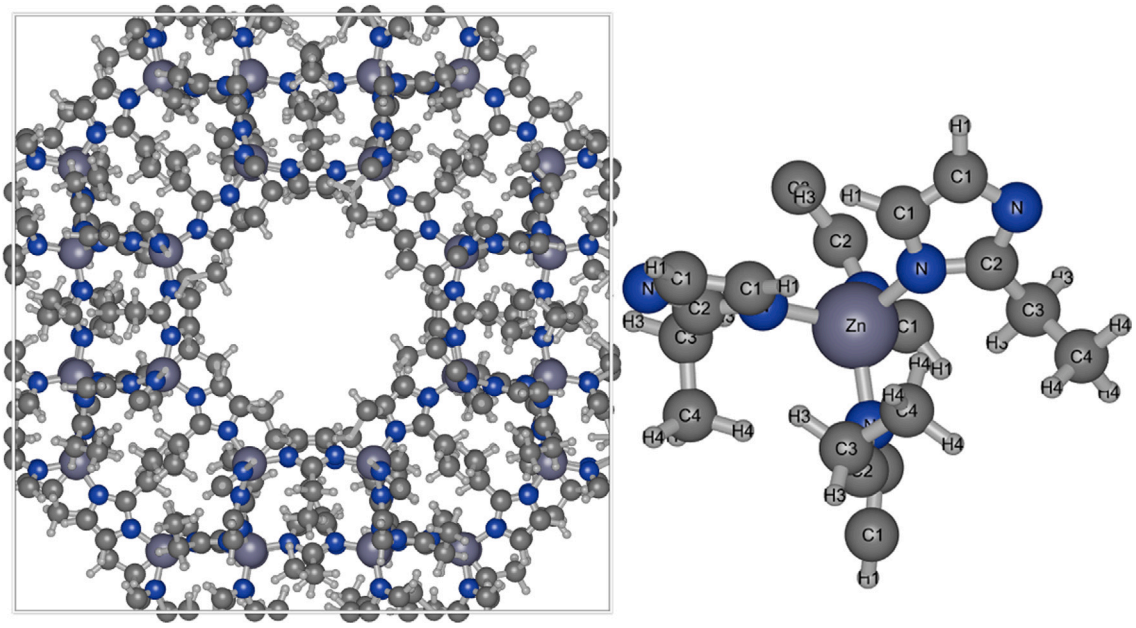

Fig. 1. Atomistic view of the unit cell of MAF-6 [12] (left) and insight on the metal centre linked to four imidazole rings (right).

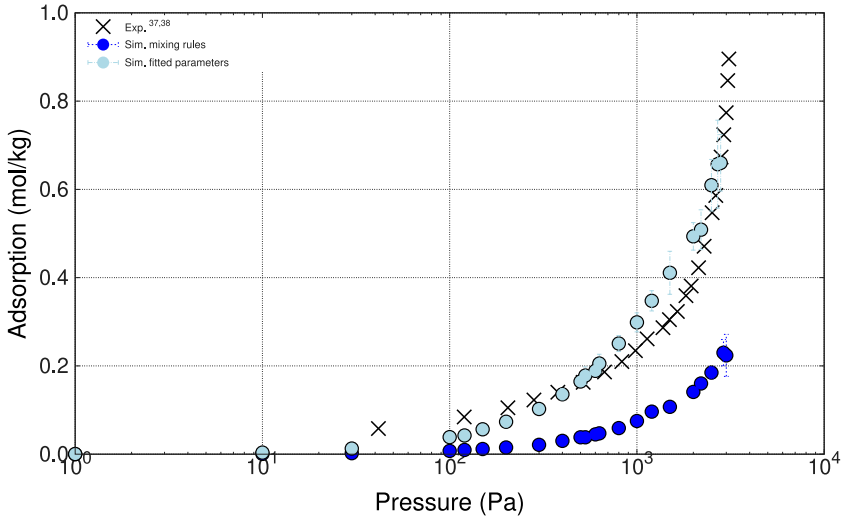

Fig. 2. Pure component water adsorption isotherms at 298 K. Comparison of experimental data [13,14] (crosses), with the calculated values using generic mixing rules (dark blue circles), and the new water-MAF L-J interaction parameters (light blue circles).

[27,28]. These modifications allow a fine-tuning of the materials for a number of applications such as selective adsorption, gas storage, energy conversion, catalysis, chemical sensors, drug delivery, bioimaging, or as light emitting materials [29–34].

A recent study, deals with the enhancement of water ingress on hydrophobic zeolitic materials applied to the recovery of alcohols from diluted aqueous solutions after alcohol/water mixture separation [35]. This work reveals that the enhancement in the water adsorption from equimolar mixtures is induced by the formation of water/alcohol clusters due to hydrogen bonding, having a moderating influence on size entropy effects. The capacity of MOFs for water adsorption is determined by combination of the available porosity of the material and the hydrophobic/hydrophilic nature of their ligand. Additional hydrogen-bonding capacity of functional groups and structural transition of the adsorbent material, also affect this property in MOFs [29,36–38].

Most work attempts to increase the stability of MOFs in water also lead to a reduction in the water adsorption capacity of the structure. Here we seek the opposite. We focus on a stable MOF and explore the possibility of improving the adsorption of water on the hydrophobic material. Improving the adsorption of water on hydrophobic materials could expand their potential applications. For example, they could be used to separate azeotropic mixtures of alcohols or to harvest water vapour from the air. As a proof of concept, we are using the MAF-6 MOF for its known hydrophobic nature. The idea is to modify the hydrophobic nature of this framework by inducing hydrophilicity to the material, using different approaches. On a first attempt we evaluate the increasing water uptake of the structure from water/alcohol mixtures. Then, we mimic the experimental procedure already used in zeolites to increase their hydrophilicity by adding cations to the structure (zeolites Z and Y), using salt as interaction centres to enhance the water adsorption capacity of MAF-6.

2. Simulation details

The adsorption properties of the material were obtained by molecular simulations. Adsorption isotherms, heats of adsorption, and Henry

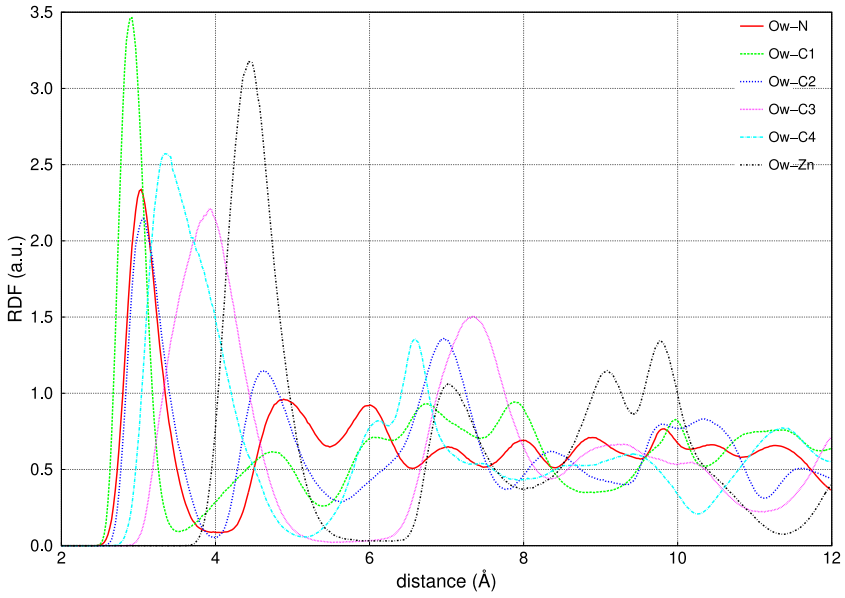

Fig. 3. Radial distribution function of the oxygen atom from water (Ow) with the atoms of the framework. Data are taken from the pure water isotherm at 3 kPa. An atomistic representation of the ligand connected to the metal centres of MAF-6 is added with the corresponding labelling of the atoms.

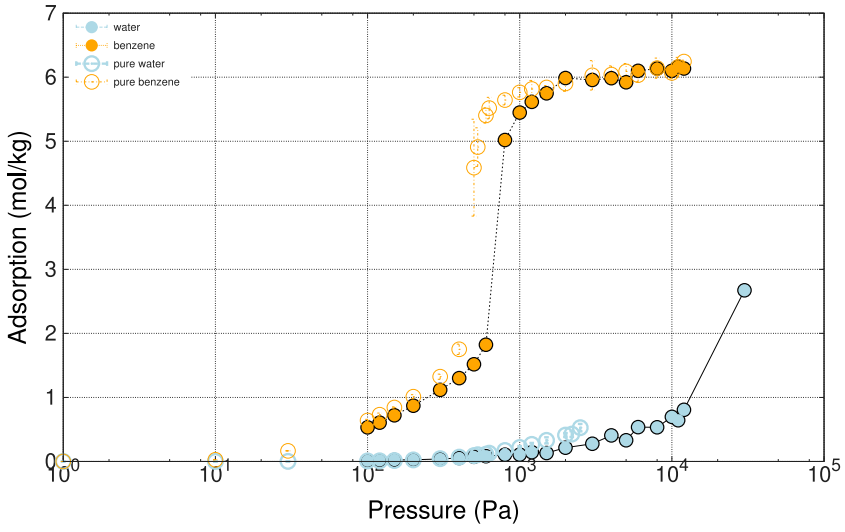

Fig. 4. Equimolar binary mixture of water (light blue full circles) with benzene (orange full circles) at 298 K. A comparison with the pure water (light blue empty circles) and pure benzene (orange empty circles) isotherms is provided.

coefficients were calculated using the software package RASPA [39,40]. Grand Canonical Monte Carlo simulations, allow computing adsorption loading for a fixed chemical potential, volume, and temperature. The Peng–Robinson equation and the fugacity coefficient relate chemical potential to pressure. Computed absolute values of adsorption (total amount of molecules within the pores) must be converted to excess adsorption (difference between the amount of gas in the system and the expected in absence of adsorption at the same temperature and pressure) [41]. To calculate heats of adsorption and Henry coefficient NVT simulations were performed in combination with the Widom test-particle method [42]. Random moves (rotation, translation, re-grow, insertion/deletion, and identity change in the case of mixtures) were applied to the molecules with at least 10^6 equilibration and 10^7 production steps to ensure equilibrium.

Lennard-Jones (L-J) and Coulombic potentials are used to define the interactions within the atoms of the system. Generic Lorentz–Berthelot mixing rules are used to compute guest–guest L-J interactions, whereas host–guest interactions are specifically defined. The Ewald summation method is employed to calculate the Coulombic interactions with a relative precision of 10^{-6}. L-J and Coulombic potentials are cut and shifted at *cutoff* distance of 12 Å.

Benzene is defined as a full atom rigid model with L-J and point charges on each atom [43]. Methanol, ethanol, and 1-propanol are modelled using TraPPE [44], where the CHx groups are considered as single interaction centres and the atoms of the hydroxyl group are defined independently. CHx groups and OH atoms have L-J and point charges, except for hydrogen atoms that only have point charges applied. We use two models previously reported for NaCl in water to describe the salt. A Kirkwood–Buff derived model (KB) [45] is compared to the one proposed by Joung and Cheatham (JC) [46] which has been used to study solubility of NaCl in water. [47] The extended simple point charge (SPC/E) model [48] is used for the water molecule as this is the most extended model on solubility studies. In the simulations involving salt, they are considered as non-framework ions, analogously to modelling cations in zeolites.

Table 1
Lennard-Jones parameters for the interaction of water with MAF-6.

	Molecule-Structure		
Atom1	Atom2	ϵ/k_B (K)	σ (Å)
N	O_{spce}	38.63	3.14
Zn	O_{spce}	48.90	2.75
$C_{1/2/3/4}$	O_{spce}	42.82	3.24
$H_{1/3/4}$	O_{spce}	17.12	2.94

We use the crystallographic position of the atoms of MAF-6 reported in the literature [12], considering the structure as a rigid framework. A representation of the unit cell of the framework and the coordination of the linkers to the metal centres is shown in Fig. 1. Following a previous work [49], all atoms of the structure have Lennard-Jones and point charges assigned. Point charges are taken from our previous work [49], and they were obtained multiplying by a factor of 1.3 these of the 2-ethylimidazole (eim) linker from a transferable set of charges already developed for ZIFs [50]. In that work, ZIFs with 2-ethylimidazole (eim) linker needed a scaling factor of 1.3 for the charges to reproduce the adsorption. As MAF-6 contains this linker we have selected this set of charges, as we did in our previous work.

Specific L-J interactions for benzene and the alcohols with the structure are taken from our previous publication [49], while in this work we provide a new set of L-J parameters for the interaction of water with the MAF-6 structure (Table 1). These L-J parameters are based on UFF [51] (metal atoms) and DREIDING [52] (remaining atoms of the structure) force fields and they were obtained by fitting pure component isotherm to experimental data. The procedure to obtain the new parameters is as follows: first L-J parameters from generic force fields are used for all atoms of the structure. Then Lorentz–Berthelot mixing rules are applied to obtain the specific interaction parameters between the model of water (SPC/E) and the atoms of the framework. Finally, these parameters are systematically modified by increasing (or decreasing) their values by a percentage. This procedure requires several iterations until we achieve a match between the experimental and simulation results.

3. Results and discussion

The main goal of this work was to figure out how to tune the hydrophobic nature of MAF-6, making it hydrophilic. To do this, the first step consisted of reproducing the water adsorption isotherm using a generic force field. We found that the generic force field could not reproduce the experimental results (Fig. 2) and therefore it was necessary to adjust the parameters. We did a readjustment of the L-J parameters for the interaction between the water molecule and the atoms of the MOF to reproduce the experimental isotherm (Fig. 2). The final parameters are listed in Table 1.

For a better understanding of the adsorption of water in this MOF, we analysed the radial distribution function (RDF) of the atom of oxygen of the molecule of water to each atom of the structure at 3 kPa. As observed in Fig. 3, the molecules of water are closer to the organic linker than to the metal centre. The main peaks for carbon atoms appear around 2.9 Å (C_1), 3.1 Å (C_2), 3.9 Å (C_3), and 3.3 Å (C_4), and around 3.0 Å for nitrogen. In all cases these are shorter distances than for the first peak corresponding to Zn (~4.4 Å). This suggests that the four imidazole rings connected to each atom of Zn act as a screen that prevents water to adsorb closer to the metal and provokes the hydrophobicity of the framework. Accordingly, we can identify two adsorption sites. One parallel to the imidazole ring (the distances O_{spce} – C_1, O_{spce} – C_2, and O_{spce} – N are similar) and a secondary site between the carbons C_3 and C_4 of the linker.

Based on these findings we could explore strategies to enhance the water adsorption in this MOF. An initial idea was to mix water with other compounds with the aim of favouring the adsorption of water. On a previous work we already studied the benzene adsorption capacity of MAF-6 and how to modify it with the presence of molecules of small alcohols [49]. The results obtained showed that for increasing chain length of the alcohol molecule, a stronger reduction on the benzene adsorption occurred. As benzene starts adsorbing at lower values of pressure than water, it was reasonable to check if that effect found for the benzene/alcohol mixtures also happens for a mixture of water and benzene. This fact was studied by analysing water adsorption from benzene/water equimolar mixture and compared with the adsorption of the single gases. This comparison is shown in Fig. 4. As can be observed, both water and benzene adsorption from the equimolar binary mixture are identical to their adsorption as pure components. This means that these gases do not influence the adsorption of each other in the structure. The gases do not compete for the same adsorption sites and therefore the presence of benzene in the framework (benzene enters

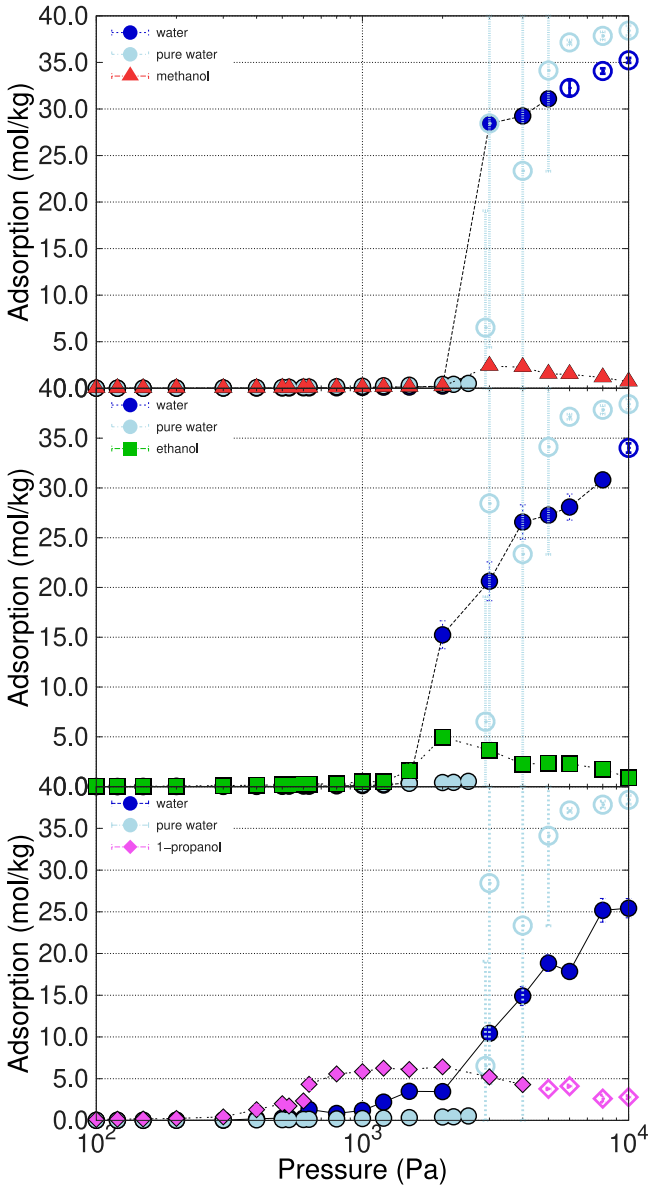

Fig. 5. Equimolar binary mixtures of water (dark blue circles) with methanol (red triangles), ethanol (green squares), and 1-propanol (pink diamonds) at 298 K. Full symbols correspond to excess adsorption while open symbols are used for absolute adsorption. A comparison with the pure water isotherm (light blue circles) is provided. The huge error bars observed between 3 kPa and 5 kPa are attributed to the phase transition of water from the gas to the liquid phase inside the pores.

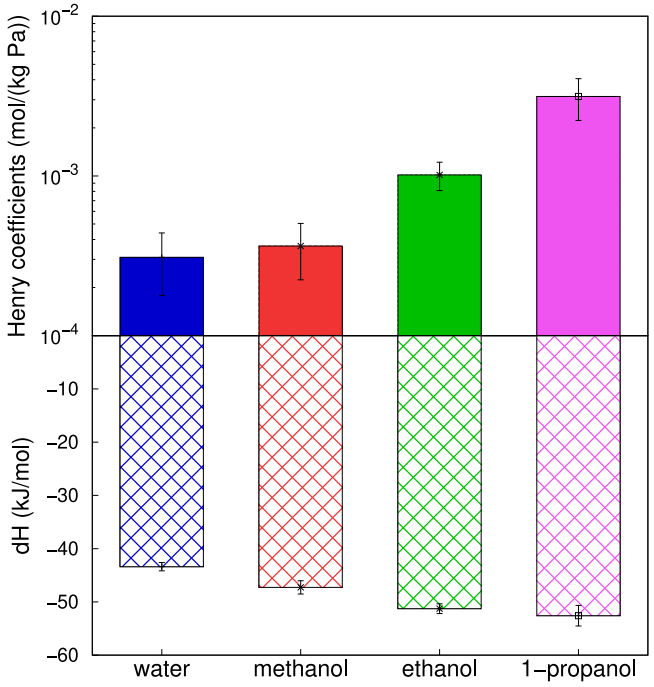

Fig. 6. Heats of adsorption (full colour bars) and Henry coefficients (bars with lattice) of water, methanol, ethanol, and 1-propanol in MAF-6 at 298 K.

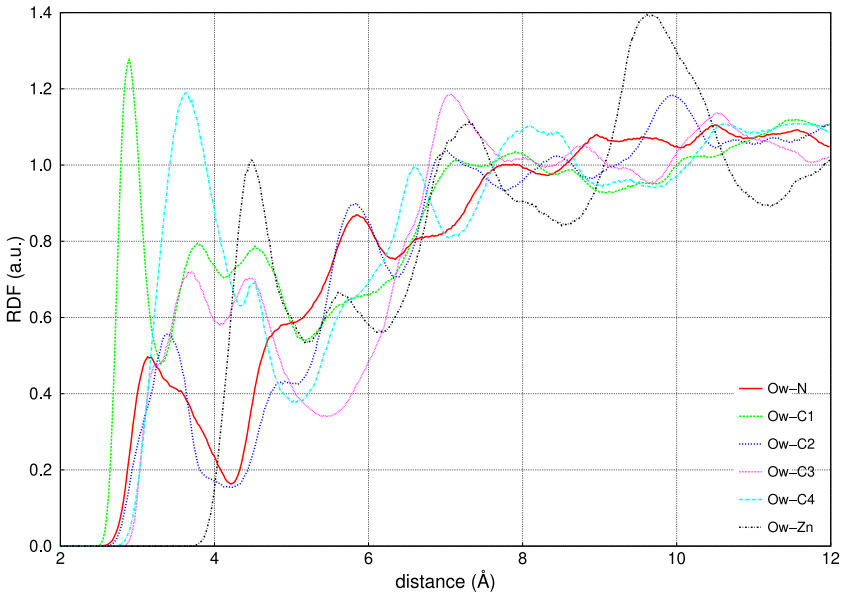

Fig. 7. Radial distribution function of the oxygen atom from water (Ow) with the atoms of the framework. Data are taken from the pure water isotherm at 5 kPa. An atomistic representation of the ligand connected to the metal centres of MAF-6 is added with the corresponding labelling of the atoms.

the structure at lower values of pressure than water) does not promote the loading of water molecules in the MOF. In our previous study, the reduction of the benzene adsorption was attributed to the molecular packing of the alcohols and the presence of alcohols hampered the adsorption of benzene. However, in this case as we are dealing with water, it is important to consider the polarity of the molecule to tune the adsorption. As shown in Fig. 4, polarity can be key on tuning water adsorption for this system. Therefore, contrary to what happened in the systems benzene/alcohols, here alcohols could promote the loading of water in the framework by acting as binding sites where water can be adsorbed. With this idea in mind, we approach the problem of creating new binding sites for water in two ways: (a) mixing water with small alcohols and (b) adding salt to the structure.

3.1. Mixtures water-alcohol

On a first approach, we investigate the effect caused by the presence of small molecules of alcohol in water adsorption. We calculate the adsorption isotherms of equimolar binary mixtures of methanol, ethanol, and 1-propanol with water at room temperature. These isotherms are shown in Fig. 5. For an easier interpretation of the water adsorption behaviour, we include a comparison with the pure component water isotherm. As can be observed from the figure, there is a phase transition of pure water from the gas to the liquid phase at about $3{\cdot}10^3$ Pa. It is for this reason that above this value of pressure, excess adsorption cannot be calculated and absolute adsorption is depicted. The huge error bars

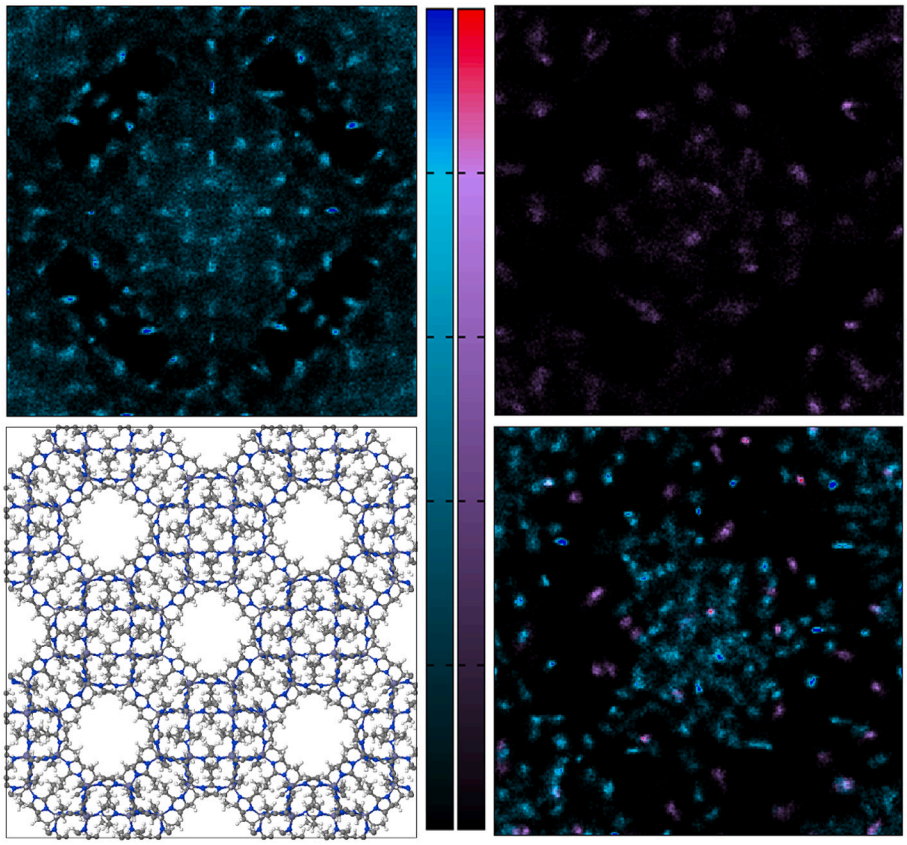

Fig. 8. Average occupation profile of water (blue) and 1-propanol (pink) as pure components (top) and from their binary mixture (bottom) at 5 kPa. Colour gradation relates with the amount of molecules. A representation of the structure is added for the sake of clarity.

observed between 3 kPa and 5 kPa are also attributed to the phase transition of water.

The phase transition occurs at higher values of pressure when water is mixed with alcohols since the partial pressure of water is lower in the mixture. Besides, we observe that the adsorption isotherm of water is smoother in the binary mixtures than as a single component, which has a stronger impact with increasing the chain length of the alcohol from the mixture. The adsorption isotherm of pure water is characterized by a pressure threshold at which the adsorption of water goes from zero to saturation. When molecules of alcohol are present, this threshold vanishes obtaining intermediate water adsorption loading before reaching the saturation capacity of the material. We also find that the starting value of pressure for the adsorption of water is reduced, being methanol, the gas with the lowest effect and 1-propanol the one with the largest. Nevertheless, 1-propanol reduces the water uptake compared to methanol or ethanol (from 30 mol/kg to 25 mol/kg of water) at the highest value of pressure (at which excess adsorption can be obtained). For all mixtures the adsorption of the alcohol is much lower than this of water (1-propanol > ethanol > methanol).

Two interesting effects happen when mixing small alcohols with water: a) the pressure at which water starts adsorbing in the structure decreases, and b) the adsorption of water becomes gradual. As a side effect, the water adsorption capacity of the MAF-6 is reduced (at the studied conditions) and this reduction is related to the length of the alcohol chain. To explain these effects we calculate the heats of adsorption and Henry coefficient. As observed from Fig. 6, the strength of the alcohol-MAF interaction follows a similar trend regarding the length of the alcohol. 1-propanol has the strongest interaction with the structure, followed by ethanol, and then methanol.

As expected, due to the hydrophobic nature of the structure, water shows the lowest values of Henry coefficient and heat of adsorption, however it is the most adsorbed molecule in all mixtures. To understand this trend we analyse the radial distribution function (RDF) of the oxygen atom of water to each atom of the structure (Fig. 7) and obtain the average occupation profile (AOP) of the mixture and the pure components (Fig. 8) at 5 kPa. As observed in Fig. 7, the first peaks for each atom are like those obtained for the pure water. The distances of water to all atoms (~2.9 Å (C_1), 3.4 Å (C_2), 3.7 and 4.4 Å C_3), and 3.6 Å (C_4), 3.1 Å (N), and Zn (~4.5 Å)), are slightly longer than in the case of the adsorption of single water. This implies that molecules tend to adsorb closer to the organic linker than to the metal centre. From our previous study [49], we know that pure alcohols exhibit the same behaviour, but the alcohol molecules are located slightly further from the carbon atoms of the imidazole ring (3.05 Å) than water molecules (2.85 Å). This suggests that both components could compete for the adsorption sites at low pressure.

At low values of pressure, the RDF of water in the mixture (not shown here) is similar to that obtained for the pure component and the same occurs with alcohols. Therefore, when the loading is low, there are enough preferential adsorption sites available for both components of the mixture, and there is no competition. However, the isotherms of the mixtures indicate that the presence of alcohols allows water to adsorb at lower values of pressure. To gain more information regarding the distribution of the guest molecules inside the structure, we study the AOPs. Fig. 8 shows AOPs of water and 1-propanol as pure components and from their equimolar binary mixture at 5 kPa.

We select this mixture as its adsorption isotherm deviates the most from the adsorption behaviour of pure water. The AOP represents the most favourable location of the adsorbed molecules, based on the projection of their centre of mass over the planes of the material. Since MAF-6 is an isotropic structure the results obtained on the *XY* plane would be analogous to these obtained on the *YZ* and *ZX* planes. As seen from the figure, the distribution of the adsorbed water molecules differs between the single component and mixtures adsorption. The

distribution of molecules from pure water adsorption is isotropic, while in the mixture the distribution is less symmetric. Contrary to water, the molecules of 1-propanol are distributed in the same way in the pure component as in mixture.

The concentration of water molecules surrounding alcohol molecules implies that interactions alcohol–water are relevant for the system. For a deeper understanding of the interactions between alcohols and water and to explain the differences on the adsorption, we analyse the formation of hydrogen bonds (HB) in the system. We define the HB formation according to a well established geometric criterion [53–56] that considers the HB between molecules when the O–O and O–H distance is less than 3.60 Å and 2.45 Å, respectively with and H–O–O angle of less than 30 degrees. Fig. 9 shows the number of hydrogen bonds (nHB) per molecule. That is, in the case of alcohol/alcohol interactions, the nHB formed is divided by the amount of alcohol molecules (same for water/water interactions). In the case of alcohol/water interactions the nHB between alcohol and water molecules is divided by the total amount of molecules present in the system.

As can be seen the nHB/molec between alcohols shows the greatest peak at about 800 Pa between 1-propanol molecules, then at 1.5 kPa for ethanol/ethanol interactions, being the nHB/molec between methanol molecules the lowest of the three at about 3 kPa. Connecting this with the decreasing trend of the heat of adsorption of the three alcohols, allows explaining the earliest adsorption of 1-propanol compared to this of ethanol and methanol. The formation of HB between molecules of alcohols together with the MAF-alcohol interaction favours the loading of alcohol molecules. In the same way, the number of HB between the alcohol and water increases with the length of the alcohol chain. The maximum number of HB is achieved at decreasing values of pressure for shorter alcohol chain length. This explains the increasing water adsorption, at lower values of pressure, in mixtures with longer chain alcohol. Finally, the largest water uptake observed from the equimolar mixture with methanol compared to this from ethanol and 1-propanol mixtures, is directly related to the water/water HB formation at the highest values of pressure. Above 1 kPa the ratio of water/water HB formed sharply rises on the mixture with methanol and ethanol while it is smoother on the 1-propanol/water mixture. This is the reason of the later phase transition of water in the last mixture. Summarizing, alcohol molecules enter the material at low pressure. These molecules act as additional adsorption sites, promoting the adsorption of water by hydrogen bonding with water molecules. Then, once some water molecules have been adsorbed, they nucleate and populate the pores. This nucleation is modulated by the available void space, which is directly related to the size and the adsorbed amount of the alcohols.

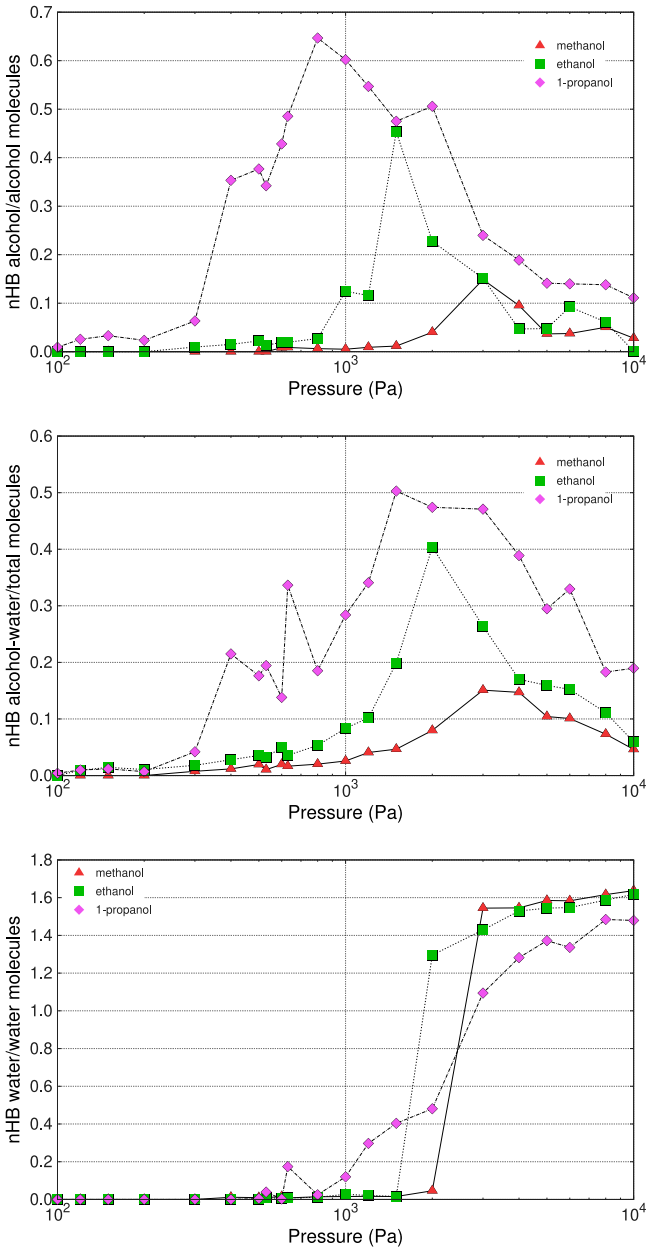

Fig. 9. Number of hydrogen bonds per molecule as a function of pressure from the equimolar binary mixtures alcohol/water. From top to bottom, comparison of the nHB/molec alcohol–alcohol, alcohol–water, and water–water. Results obtained from the mixture with methanol, ethanol, and 1-propanol are represented by red squares, green circles, and pink triangles, respectively.

3.2. Salt in the structure

The second approach is the addition of small weight percentages of NaCl to the structure. This is similar to the process used to make many zeolites hydrophilic: using cations which act as strong interaction sites with water. We use two salt models from the literature [45,46] and compute water adsorption isotherms varying the concentration of salt. In this way, we can study the influence of the salt on the adsorption of water and compare the performance of the models.

Fig. 10 shows the calculated adsorption. Overall, the results obtained with both models are similar. At values of pressure lower than 10^3 Pa the loading of water increases with the percentage of salt in the structure, while above this pressure we observe the opposite behaviour (lower adsorption for higher concentration of salt). In the low pressure range, it is worth noting that the use of the Joung and Cheatham model leads to a significant increase of water adsorption with 10 wt% or 10% vy weight (often stated 10% w/w) of salt compared to 8 wt% of salt. On the other hand, when using the Kirkwood–Buff model, there is an unexpected increase of water loading with 6 wt% of salt. From these results we deduce that the presence of NaCl creates additional adsorption sites for water enhancing its adsorption at values of pressure below 10^3 Pa, while above this value NaCl occupies the available space, reducing therefore the adsorption of water. Analysing the water/water HB formation in the same way as we did before (Fig. 11), it seems clear that the presence of salt enhances the formation of HB between water molecules. Above 10 kPa both NaCl models lead to the same amount of nHB/molec with a small reduction of this ratio for increasing concentration of salt in the system.

At 1 kPa the ratio varies from 1.3 to 1.5 for all weight percentages of NaCl except for 2 wt% that shows the lowest value (0.8–1 nHB/molec), being all of them a great improvement compared to pure water adsorption. At the lowest value of pressure, there is still an increase on the HB formation, but not as large as for 1 kPa. At 100 Pa, the difference between models is quite remarkable for the different weight

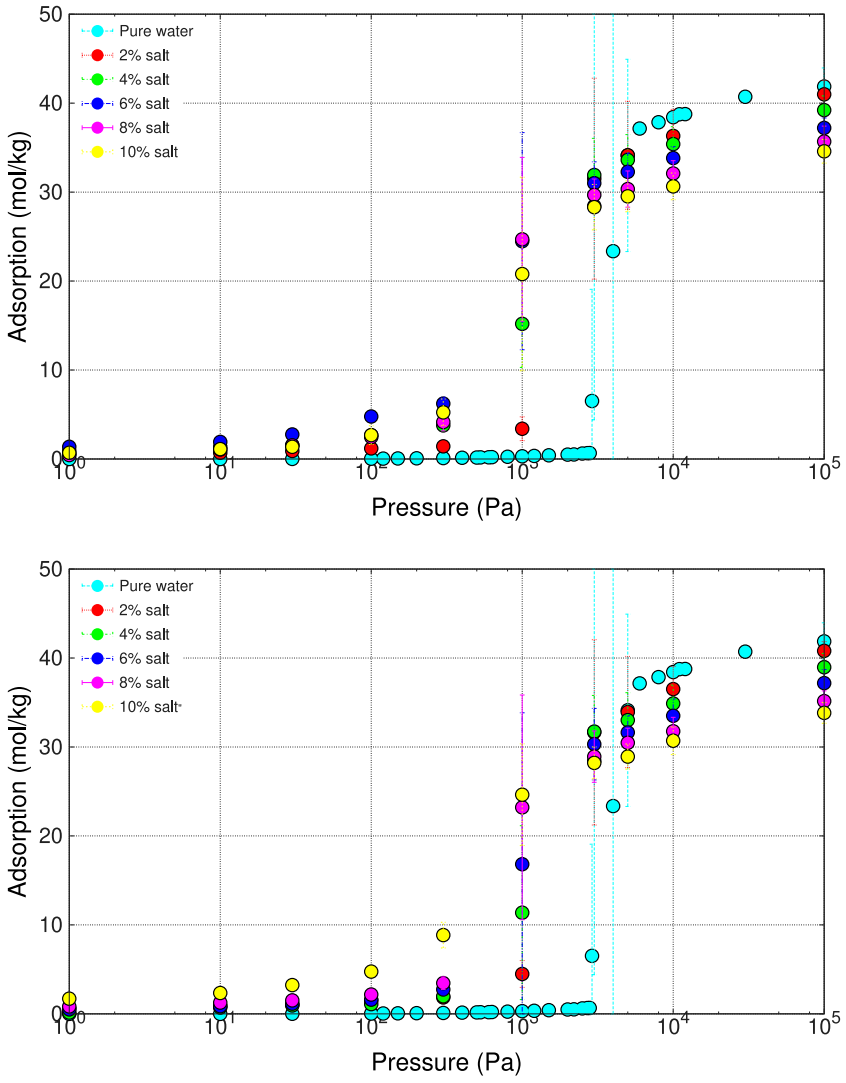

Fig. 10. Water adsorption isotherms in MAF-6 at 298 K with different weight percentages of NaCl using the Joung and Cheatham model (top) and the Kirkwood–Buff derived model (bottom).

percentages of NaCl studied (except 2% by weight). The results of the JC-model show the highest amount of nHB/molec (between 0.4 and 0.8), this together with the trends of the adsorption isotherms, and the fact that this model has been widely used for NaCl in water solubility studies, lead us to trust these results more than those obtained with the KB-model. In summary, our results show that adding a 10 wt% of salt to the structure improves the adsorption of water in the MAF-6 in such a way the water molecules can enter the structure at low pressure (below 100 Pa). As a counterpart the saturation capacity of the material is reduced from 40 mol/kg to 34 mol/kg. By varying the weight percentage of salt we can modulate the decrease in the saturation capacity as well as the change in the pressure at which the water begins to adsorb. We have seen that both approaches (alcohol and salt additions) turn the MAF-6 into a more hydrophilic material, allowing the adsorption of water at lower values of pressure than in the bare structure. At the same time, the saturation capacity is reduced. For the case of mixtures with alcohols, propanol induces the greatest decrease, obtaining a saturation capacity of 25 mol/kg. Ethanol and methanol practically do not reduce the saturation capacity of the structure and the effect is similar to that obtained by adding a 2 wt% and 4 wt% of salt. The maximum percentage of salt that we have tested leads to a saturation capacity of 30 mol/kg. With alcohols, the value of pressure at which water starts entering the framework is higher than 1 kPa, while with the addition of salt we observe water adsorption below 100 Pa. Finally, the maximum water enhancement is found to be about 25 mol/kg in presence of 10 wt% of NaCl at 1 kPa.

4. Conclusions

With the idea of modifying the hydrophobicity of MAF-6, we have used two approaches. The first one dealt with the effect that the presence of small alcohols (methanol, ethanol, and 1-propanol) has on the water adsorption from equimolar binary mixtures alcohol/water. The second approach was to evaluate the influence of different weight percentages of salt on the adsorption capacity of the material. For this purpose, using molecular simulation we calculated adsorption isotherms, heats of adsorption, radial distribution functions, average occupation profiles, and hydrogen bonds formation. From water/alcohol mixtures analysis we observed that although there is no direct competition between the molecules with the structure, the presence of alcohol in the mixture favours the adsorption of water at low pressure. Alcohols are adsorbed at lower values of pressure than water, acting as additional adsorption sites for the latter. Furthermore, the larger the size of the alcohol, the earlier adsorption of the molecules from the mixture. The water phase transition is postponed in presence of 1-propanol, this phenomenon having a direct relation with the formation of hydrogen bonds. The addition of certain amounts of salt also creates

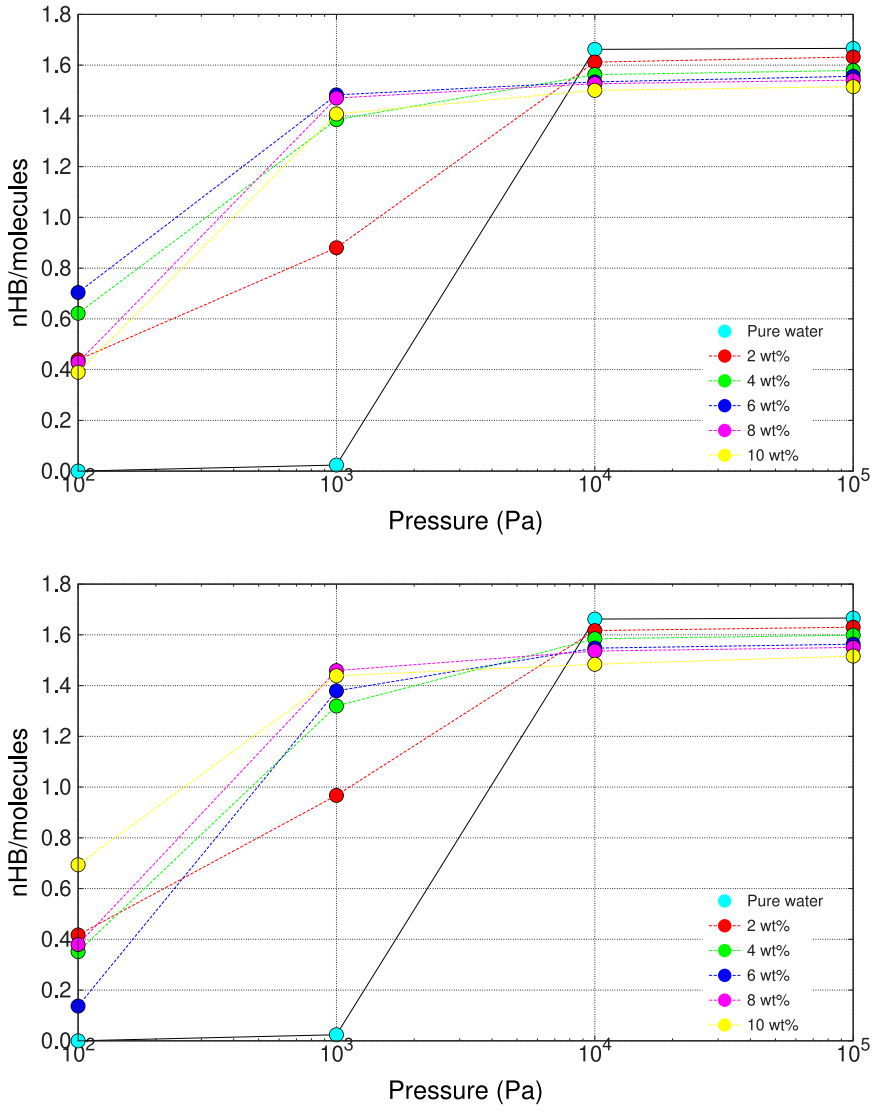

Fig. 11. Number of hydrogen bonds per molecule as a function of pressure from the water adsorption in presence of NaCl. Comparison of the results obtained for the addition of 2 wt% (green), 4 wt% (dark blue), 6 wt% (pink), 8 wt% (light blue), 10 wt% (yellow) of salt. Data from the JC- (top) and the KB-model (bottom) are represented by squares and circles, respectively. Black triangles show the results from the pure component water adsorption.

additional adsorption sites for water favouring its adsorption, with the counterpart of reducing the maximum water uptake. On a similar way as already happened with zeolites, this mechanism could guide experimental groups to develop MOFs with cations. Both approaches lead to higher water adsorption of MAF-6 by giving optimal conditions for a smooth phase transition of water when it is confined in the structure of MAF-6.

Declaration of competing interest

The authors declare that they have no known competing financial interests or personal relationships that could have appeared to influence the work reported in this paper.

Acknowledgements

This work was supported by the Spanish Ministerio de Ciencia, Innovación y Universidades (CTQ2017-92173-EXP, PCIN-2017-102, PID2019-111189GBI00, IJC2018-038162-I, and IJC2019-042207-I). We thank C3UPO for the HPC support.

References

[1] M.R. Benzigar, S.N. Talapaneni, S. Joseph, K. Ramadass, G. Singh, J. Scaranto, U. Ravon, K. Al-Bahily, A. Vinu, Recent advances in functionalized micro and mesoporous carbon materials: synthesis and applications, Chem. Soc. Rev. 47 (2018) 2680–2721.

[2] C. Liang, Z. Li, S. Dai, Mesoporous carbon materials: Synthesis and modification, Angew. Chem., Int. Ed. Engl. 47 (20) (2008) 3696–3717.

[3] T. Kyotani, Synthesis of various types of nano carbons using the template technique, Bull. Chem. Soc. Japan 79 (9) (2006) 1322–1337.

[4] M. Inagaki, Y.A. Kim, M. Endo, Graphene: preparation and structural perfection, J. Mater. Chem. 21 (2011) 3280–3294.

[5] M. Inagaki, M. Toyoda, T. Tsumura, Control of crystalline structure of porous carbons, RSC Adv. 4 (2014) 41411–41424.

[6] V. Malgras, Q. Ji, Y. Kamachi, T. Mori, F.-K. Shieh, K.C.-W. Wu, K. Ariga, Y. Yamauchi, Templated synthesis for nanoarchitectured porous materials, Bull. Chem. Soc. Japan 88 (9) (2015) 1171–1200.

[7] H. Figueiredo, C. Quintelas, Tailored zeolites for the removal of metal oxyanions: Overcoming intrinsic limitations of zeolites, J. Hard Mater. 274 (2014) 287–299.

[8] V. Valtchev, G. Majano, S. Mintova, J. Pérez-Ramírez, Tailored crystalline microporous materials by post-synthesis modification, Chem. Soc. Rev. 42 (2013) 263–290.

[9] J.D. Rimer, M. Kumar, R. Li, A.I. Lupulescu, M.D. Oleksiak, Tailoring the physicochemical properties of zeolite catalysts, Catal. Sci. Technol. 4 (2014) 3762–3771.

[10] Y. Wei, T.E. Parmentier, K.P. de Jong, J. Zečević, Tailoring and visualizing the pore architecture of hierarchical zeolites, Chem. Soc. Rev. 44 (2015) 7234–7261.
[11] M. Shamzhy, M. Opanasenko, P. Concepción, A. Martínez, New trends in tailoring active sites in zeolite-based catalysts, Chem. Soc. Rev. 48 (2019) 1095–1149.
[12] X.-C. Huang, Y.-Y. Lin, J.-P. Zhang, X.-M. Chen, Ligand-directed strategy for zeolite-type metal–organic frameworks: Zinc(II) imidazolates with unusual zeolitic topologies, Angew. Chem., Int. Ed. Engl. 45 (10) (2006) 1557–1559.
[13] C.-T. He, L. Jiang, Z.-M. Ye, R. Krishna, Z.-S. Zhong, P.-Q. Liao, J. Xu, G. Ouyang, J.-P. Zhang, X.-M. Chen, Exceptional hydrophobicity of a large-pore metal–organic zeolite, J. Am. Chem. Soc. 137 (22) (2015) 7217–7223.
[14] M. Gao, J. Wang, Z. Rong, Q. Shi, J. Dong, A combined experimental-computational investigation on water adsorption in various ZIFs with the SOD and RHO topologies, RSC Adv. 8 (2018) 39627–39634.
[15] O.M. Yaghi, G. Li, H. Li, Selective binding and removal of guests in a microporous metal-organic framework, Nature 378 (6558) (1995) 703–706.
[16] G. Férey, Microporous solids: From organically templated inorganic skeletons to hybrid frameworks...ecumenism in chemistry, Chem. Mater. 13 (10) (2001) 3084–3098.
[17] N. Stock, S. Biswas, Synthesis of metal-organic frameworks (MOFs): Routes to various mof topologies, morphologies, and composites, Chem. Rev. 112 (2) (2012) 933–969.
[18] L. Ji, J. Hao, K. Wu, N. Yang, Potential-tunable metal–organic frameworks: Electrosynthesis, properties, and applications for sensing of organic molecules, J. Phys. Chem. C 123 (4) (2019) 2248–2255.
[19] B. Liu, K. Vellingiri, S.-H. Jo, P. Kumar, Y.S. Ok, K.-H. Kim, Recent advances in controlled modification of the size and morphology of metal-organic frameworks, Nano Res. 11 (9) (2018) 4441–4467.
[20] D. Kim, M. Kang, H. Ha, C.S. Hong, M. Kim, Multiple functional groups in metal–organic frameworks and their positional regioisomerism, Coord. Chem. Rev. 438 (2021) 213892.
[21] S.J. Garibay, S.M. Cohen, Isoreticular synthesis and modification of frameworks with the uio-66 topology, Chem. Commun. 46 (2010) 7700–7702.
[22] A.D. Burrows, C.G. Frost, M.F. Mahon, C. Richardson, Post-synthetic modification of tagged metal–organic frameworks, Angew. Chem., Int. Ed. Engl. 47 (44) (2008) 8482–8486.
[23] T. Li, M.T. Kozlowski, E.A. Doud, M.N. Blakely, N.L. Rosi, Stepwise ligand exchange for the preparation of a family of mesoporous MOFs, J. Am. Chem. Soc. 135 (32) (2013) 11688–11691.
[24] S. Das, H. Kim, K. Kim, Metathesis in single crystal: Complete and reversible exchange of metal ions constituting the frameworks of metal-organic frameworks, J. Am. Chem. Soc. 131 (11) (2009) 3814–3815.
[25] D. Sun, W. Liu, M. Qiu, Y. Zhang, Z. Li, Introduction of a mediator for enhancing photocatalytic performance via post-synthetic metal exchange in metal–organic frameworks (MOFs), Chem. Commun. 51 (2015) 2056–2059.
[26] C. Liu, N.L. Rosi, Ternary gradient metal–organic frameworks, Faraday Discuss. 201 (2017) 163–174.
[27] S. Yuan, W. Lu, Y.-P. Chen, Q. Zhang, T.-F. Liu, D. Feng, X. Wang, J. Qin, H.-C. Zhou, Sequential linker installation: Precise placement of functional groups in multivariate metal–organic frameworks, J. Am. Chem. Soc. 137 (9) (2015) 3177–3180.
[28] S. Yuan, Y.-P. Chen, J.-S. Qin, W. Lu, L. Zou, Q. Zhang, X. Wang, X. Sun, H.-C. Zhou, Linker installation: Engineering pore environment with precisely placed functionalities in zirconium MOFs, J. Am. Chem. Soc. 138 (28) (2016) 8912–8919.
[29] S. Chaemchuen, X. Xiao, N. Klomkliang, M.S. Yusubov, F. Verpoort, Tunable metal–organic frameworks for heat transformation applications, Nanomaterials 8 (661) (2018).
[30] C. Wang, D. Liu, W. Lin, Metal–organic frameworks as a tunable platform for designing functional molecular materials, J. Am. Chem. Soc. 135 (36) (2013) 13222–13234.
[31] W. Lu, Z. Wei, Z.-Y. Gu, T.-F. Liu, J. Park, J. Park, J. Tian, M. Zhang, Q. Zhang, T. Gentle III, M. Bosch, H.-C. Zhou, Tuning the structure and function of metal–organic frameworks via linker design, Chem. Soc. Rev. 43 (2014) 5561–5593.
[32] Q. Wang, J. Bai, Z. Lu, Y. Pan, X. You, Finely tuning MOFs towards high-performance post-combustion CO2 capture materials, Chem. Commun. 52 (2016) 443–452.
[33] J.P. Dürholt, B.F. Jahromi, R. Schmid, Tuning the electric field response of MOFs by rotatable dipolar linkers, ACS Central Sci. 5 (8) (2019) 1440–1448.
[34] E. Whelan, F.W. Steuber, T. Gunnlaugsson, W. Schmitt, Tuning photoactive metal–organic frameworks for luminescence and photocatalytic applications, Coord. Chem. Rev. 437 (2021) 213757.
[35] R. Krishna, J.M. van Baten, Water/alcohol mixture adsorption in hydrophobic materials: Enhanced water ingress caused by hydrogen bonding, ACS Omega 5 (43) (2020) 28393–28402.
[36] P.M. Schoenecker, C.G. Carson, H. Jasuja, C.J.J. Flemming, K.S. Walton, Effect of water adsorption on retention of structure and surface area of metal–organic frameworks, Ind. Eng. Chem. Res. 51 (18) (2012) 6513–6519.
[37] G.E. Cmarik, M. Kim, S.M. Cohen, K.S. Walton, Tuning the adsorption properties of UiO-66 via ligand functionalization, Langmuir 28 (44) (2012) 15606–15613.
[38] H. Jasuja, J. Zang, D.S. Sholl, K.S. Walton, Rational tuning of water vapor and CO2 adsorption in highly stable Zr-based MOFs, J. Phys. Chem. C 116 (44) (2012) 23526–23532.
[39] D. Dubbeldam, S. Calero, D.E. Ellis, R.Q. Snurr, RASPA: molecular simulation software for adsorption and diffusion in flexible nanoporous materials, Mol. Simul. 42 (2) (2016) 81–101.
[40] D. Dubbeldam, A. Torres-Knoop, K.S. Walton, On the inner workings of Monte Carlo codes, Mol. Simul. 39 (14–15) (2013) 1253–1292.
[41] T. Duren, R.Q. Snurr, Assessment of isoreticular metal-organic frameworks for adsorption separations: A molecular simulation study of methane/n-butane mixtures, J. Phys. Chem. B 108 (40) (2004) 15703–15708.
[42] B. Widom, Some topics in the theory of fluids, J. Chem. Phys. 39 (1963) 2808–2812.
[43] N. Rai, J.I. Siepmann, Transferable potentials for phase equilibria. 9. Explicit hydrogen description of benzene and five-membered and six-membered heterocyclic aromatic compounds, J. Phys. Chem. B 111 (36) (2007) 10790–10799.
[44] B. Chen, J.J. Potoff, J.I. Siepmann, Monte Carlo calculations for alcohols and their mixtures with alkanes. transferable potentials for phase equilibria. 5. United-atom description of primary, secondary, and tertiary alcohols, J. Phys. Chem. B 105 (15) (2001) 3093–3104.
[45] S. Weerasinghe, P.E. Smith, A Kirkwood–Buff derived force field for sodium chloride in water, J. Chem. Phys. 119 (21) (2003) 11342–11349.
[46] I.S. Joung, T.E. Cheatham, Determination of alkali and halide monovalent ion parameters for use in explicitly solvated biomolecular simulations, J. Phys. Chem. B 112 (30) (2008) 9020–9041.
[47] J.L. Aragones, E. Sanz, C. Vega, Solubility of NaCl in water by molecular simulation revisited, J. Chem. Phys. 136 (2012) 244508.
[48] H.J.C. Berendsen, J.R. Grigera, T.P. Straatsma, The missing term in effective pair potentials, J. Phys. Chem. 91 (24) (1987) 6269–6271.
[49] A. Martin-Calvo, J.J. Gutierrez-Sevillano, D. Dubbeldam, S. Calero, Using aliphatic alcohols to tune benzene adsorption in MAF-6, Adv. Theory Simul. 2 (11) (2019) 1900112.
[50] J.J. Gutierrez-Sevillano, S. Calero, C.O. Ania, J.B. Parra, F. Kapteijn, J. Gascon, S. Hamad, Toward a transferable set of charges to model zeolitic imidazolate frameworks: Combined experimental–theoretical research, J. Phys. Chem. C 117 (1) (2013) 466–471.
[51] A.K. Rappe, C.J. Casewit, K.S. Colwell, W.A. Goddard, W.M. Skiff, UFF, a full periodic table force field for molecular mechanics and molecular dynamics simulations, J. Am. Chem. Soc. 114 (25) (1992) 10024–10035.
[52] S.L. Mayo, B.D. Olafson, W.A. Goddard, DREIDING: a generic force field for molecular simulations, J. Phys. Chem. 94 (26) (1990) 8897–8909.
[53] A. Luzar, D. Chandler, Structure and hydrogen bond dynamics of water-dimethyl sulfoxide mixtures by computer simulations, J. Chem. Phys. 98 (10) (1993) 8160–8173.
[54] J. Martí, J.A. Padro, E. Guàrdia, Molecular dynamics simulation of liquid water along the coexistence curve: Hydrogen bonds and vibrational spectra, J. Chem. Phys. 105 (2) (1996) 639–649.
[55] J. Martí, Analysis of the hydrogen bonding and vibrational spectra of supercritical model water by molecular dynamics simulations, J. Chem. Phys. 110 (14) (1999) 6876–6886.
[56] S. Calero, P. Gómez-Alvarez, Effect of the confinement and presence of cations on hydrogen bonding of water in LTA-type zeolite, J. Phys. Chem. C 118 (17) (2014) 9056–9065.